Bioactive Materials 25 (2023) 73–85

Contents lists available at ScienceDirect

Bioactive Materials

journal homepage: www.keaipublishing.com/en/journals/bioactive-materials

The combination of eddy thermal effect of biodegradable magnesium with immune checkpoint blockade shows enhanced efficacy against osteosarcoma

Jun Ge [a,b,1], Nailin Yang [b,1], Yuqi Yang [b,1], Hao Yu [a], Xiaoyuan Yang [b], Yingjie Wang [a], Tianyi Wang [c], Shuning Cheng [b], Yuanjie Wang [b], Zhihui Han [b], Yun Teng [a], Jun Zou [a,***], Huilin Yang [a,**], Liang Cheng [b,*]

[a] Department of Orthopedic Surgery, The First Affiliated Hospital of Soochow University, Suzhou, Jiangsu, China
[b] Institute of Functional Nano & Soft Materials (FUNSOM), Jiangsu Key Laboratory for Carbon-Based Functional Materials & Devices, Soochow University, Suzhou, Jiangsu, China
[c] Department of Neurosurgery, The First Affiliated Hospital of Soochow University, Suzhou, Jiangsu, China

ARTICLE INFO

Keywords:
Osteosarcoma
Eddy thermal effect
Magnesium rods (MgR)
Osteosarcoma therapy
Tumor microenvironment (TME)
immunotherapy

ABSTRACT

Osteosarcoma (OS) patients have a poor prognosis due to its high degree of heterogeneity and high rate of metastasis. Magnetic hyperthermia therapy (MHT) combined with immunotherapy is an effective strategy to treat solid and metastatic tumors. Here, we combined biodegradable magnesium (Mg) macroscale rods, which acted as an eddy thermo-magnetic agent under a low external alternating magnetic field, and immunotherapy to achieve a radical cure for OS. The eddy thermal effect (ETE) of the Mg rods (MgR) showed outstanding cytotoxic effects and enhanced the maturation of dendritic cells (DCs), and the mild MHT induced the immunogenic cell death (ICD) in the OS cells. Combined with immune checkpoint blockade (ICB) therapy, we obtained an excellent curative effect against OS, and a further evaluation demonstrated that the local MHT induced by the MgR increased T cells infiltration and the polarization of M1 macrophages. Interestingly, the biodegradable MgR also promoted bone osteogenesis. Our work highlighted the uneven ETE mediated by the biodegradable MgR induced a comprehensive immunologic activation in the OS tumor microenvironment (TME), which would inspire the application of MHT for the effective treatment of OS.

1. Introduction

Osteosarcoma (OS) is the most common type of malignant tumor in the bone [1]. The treatment for OS is still challenging due to the poor efficacy of the currently available therapeutics, high rate of metastasis and low long-term survival rate of the patients. Since the introduction of neoadjuvant chemotherapy in the 1970s, the five-year survival rate for OS patients has increased to 50%. However, the prognosis of OS patients has remained unchanged for decades [2,3]. The high degree of heterogeneity of OS poses a major hurdle for the development of molecular-targeted therapies [4]. Besides, the side effects of radical surgical resection and systemic chemotherapy, including significant systemic symptoms, drug resistance, uncontrollable metastasis, and critical bone defects, affect the quality of life of OS patients [5]. According to the available guidelines for OS treatment worldwide [6–8], only the OS patients with early-stage disease or chemotherapy sensitivity could be exempted from radical amputation or wide excision. Limb salvage has also greatly relieved the mental burden of OS patients. Therefore, it is highly urgent to develop a kind of highly efficient and advanced therapeutic strategy to both cure OS with limb salvage and protect the bone from cancer-induced destruction.

Recently, hyperthermia therapy has drawn a wide attention owing to

Peer review under responsibility of KeAi Communications Co., Ltd.
* Corresponding author.
** Corresponding author.
*** Corresponding author.
E-mail addresses: jzou@suda.edu.cn (J. Zou), hlyang@suda.edu.cn (H. Yang), lcheng2@suda.edu.cn (L. Cheng).
[1] These authors contributed equally to the work.

https://doi.org/10.1016/j.bioactmat.2023.01.008
Received 25 October 2022; Received in revised form 2 January 2023; Accepted 12 January 2023

its low toxicity to the host, low therapeutic resistance as well as reliable efficacy [9]. Among the different hyperthermia treatments, magnetic hyperthermia therapy (MHT) is a potential option for treating solid tumors. Under an external alternating magnetic field (AMF), the magnetothermal agents could generate large amounts of heat to induce cytotoxic effects on the tumor [10]. Compared with other hyperthermia methods, MHT has the unique advantage of high tissue-penetration [11,12]. Therefore, magnetic nanoparticles (MNPs) have become the primary choice MHT of tumors. However, the low efficacy and poor stability of MNPs limit their application in the clinic [13,14]. Different from the heating power relaxation loss in MNPs, the bulk metal conductors with small resistivity induce an eddy thermal effect (ETE) under AMF. According to the Faraday's law of electromagnetic induction, when an alternating current is applied in the coil, an AMF is generated inside it. The eddy current electric field generated by AMF further induces a closing circuit and thermal effect on the conductor in the coil

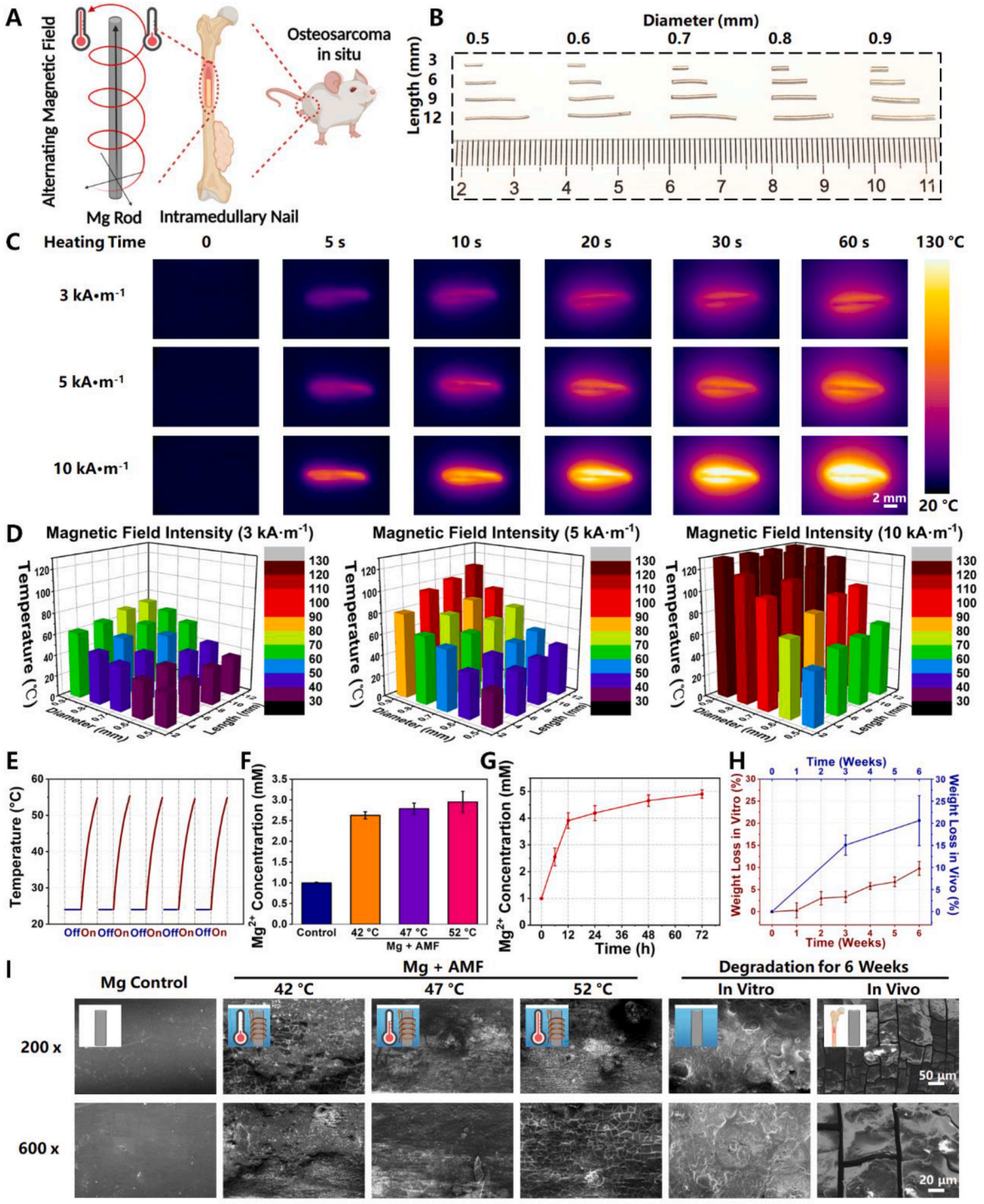

Fig. 1. Eddy thermal effects of magnesium rods. **A.** Schematic illustration for the eddy thermal therapy of MgR on OS. **B.** The general photograph of MgR. **C.** The eddy thermal images of the MgR under AMF. **D.** The temperature of the ETE depends on the magnetic field intensity, MgR diameter and MgR length. **E.** Heating cycle of the MgR under 5 kA · m^{-1} AMF. Heating time: 20 s. **F.** Mg ions released from MgR under AMF. **G.** Mg ions released from MgR in high glucose-medium (N = 3). **H.** Weight loss of MgR *in vitro* and *in vivo* for 6 weeks (N = 6). **I.** SEM images of MgR. The diameter and the length of MgR is 0.7 mm and 9 mm.

[15]. Importantly, the bulk metal conductors show a much higher magnetothermal efficiency and a higher stability in comparison with the previously reported MNPs. Among the various macro metallic materials, magnesium (Mg), featuring low electrical conductivity [16], superb biocompatibility along with bone regeneration ability [17], is an excellent candidate for MHT of OS.

Nevertheless, the local application of MHT did not reduce the high recurrence and metastasis rates associated with OS to a large extent. Thus, combinatory therapy based on MHT has become emerged as an effective strategy to treat tumors radically [9]. Recently, the efficacy of immunotherapy has garnered extensive attention [18,19]. A large number of pre-clinical experiments have demonstrated the optimal therapeutic efficacy of immunotherapy in many types of tumors including OS [20,21]. It is even more inspiring that immunotherapy has been reported to effectively inhibit tumor metastasis and recurrence [22]. Regrettably, single immunotherapy often fails to achieve an ideal efficacy due to the immunosuppressive microenvironment and immune escape mechanism of tumors [23]. Famous for its immune inertia, OS is considered as a 'cold tumor'. Transforming the immune microenvironment of OS from 'cold tumor' to 'hot tumor' might be a potential strategy to enhance the therapeutic efficacy of cancer immunotherapy [24]. On the one hand, the dying tumor cells could produce tumor-associated antigens, leading to the activation of tumor specific immune responses, and on the other hand, MHT could further promote immune cell infiltration, thus creating a pro-inflammatory tumor microenvironment.

Herein, we employed biodegradable Mg macroscale rods as an eddy thermo-magnetic agent under low field intensity AMF and combined it with immunotherapy to achieve a radical cure for OS for the first time. The ETE of the MgR showed excellent cytotoxic effects on OS cells *in vitro*. Further analyses revealed the comprehensive immunogenic activation mediated by the uneven ETE induced by the MgR on both OS cells and the TME. Combined with immune checkpoint blockage (ICB) therapy, there was a further augmentation of the therapeutic efficacy against OS cells and tumors. Moreover, the evaluation of the immune phenotype also suggested that the local MHT mediated by the MgR enhanced T cells infiltration and M1 polarization of macrophages. More importantly, the biodegradable MgR promoted bone osteogenesis. The current work revealed the comprehensive immunological activation induced by the uneven ETE heating in the TME and the reliable translation potential of the biodegradable MgR in OS therapy.

2. Results and discussion

2.1. Eddy thermal effects of the degradable Mg rods

ETE is a heating effect mainly caused by a closed circuit in a conductor under an external AMF (Fig. 1A). The size of the conductor material and the intensity of the AMF largely affect the efficiency of ETE. Magnesium rods (MgR, Fig. S1) with different lengths (L: 3, 6, 9, and 12 mm) and diameters (D: 0.5, 0.6, 0.7, 0.8, and 0.9 mm) were measured under AMF with different intensities (Happl × Fappl = n kA · M^{-1}, n = 3, 5, and 10) (Fig. 1B). It was found that the MgR induced rapid thermal effect under AMF. For example, MgR (D = 0.7 mm, L = 9 mm) could be quickly heated from 24 °C to 130 °C within 1 min under an AMF of 10 kA · m^{-1} (Fig. 1C), and the results indicated that the intensity of the AMF and the geometry of the MgR were directly proportional to the ETE. Furthermore, the change in the diameter had a greater impact on the heating performance than the change in the length of the MgR (Fig. 1D). As expected, the MgR also showed good magnetocaloric stability for ETE treatment after five cycles of heating (Fig. 1E). In addition, the heating performance of MgR in PBS solution was evaluated. MgR could be heated from room temperature to more than 50 °C under an AMF of 10 kA · M^{-1} within 5 min. An outstanding magnetothermal efficiency of MgR was further verified compared with the same mass of Fe_3O_4 NPs, a kind of common nano-magnetothermal agent (Fig. S2). Above all, the outstanding ETE and stability of the MgR under the AMF provided a solid rationale for their application as MHT agents for treating OS.

Additionally, Mg ions released from the MgR were also higher under ETE (Fig. 1F). Further analytical chemistry results indicated that the ETE process did not dramatically accelerate the degradation of the Mg rods or cause the release of large amounts of hydrogen (Figs. S3–4). Several MgR (D = 0.7 mm, L = 9 mm) were soaked in serum-free high glucose medium at 37 °C for different duration (0, 6, 12, 24, 48, and 72 h), and the data showed that the content of Mg^{2+} increased over time, suggesting that the MgR were continuously degraded in such a solution and reached to 5 mM after 72 h incubation (Fig. 1G). Then, the MgR (D = 0.7 mm, L = 9 mm) were incubated in Hanks simulated body fluid at 37 °C to simulate its degradation. It was found that the mass of the MgR decreased gradually over time, with a loss of about 10% after 6 weeks of immersion (Fig. 1H). After their implantation in the femur of mice for 6 weeks, the loss of weight of the MgR was close to 20% (Fig. 1I), mostly excreted via urine [25], indicating a stronger *in vivo* biodegradation that could be utilized to promote bone osteogenesis (Fig. 1H). Additionally, the morphology of MgR with different treatments was also characterized by scanning electron microscopy (SEM). After AMF application, the surface of MgR became rougher because of the ETE. As the reaction temperature increased, the cracks on the surface simultaneously increased to a certain extent. Compared with the original surface, the surface of MgR after soaking or implanting in the body of the mice for 6 weeks was rough and uneven, further confirming its bio-degradation (Fig. 1I).

2.2. Magnetic hyperthermia mediated by MgR for osteosarcoma

Next, the *in vitro* efficacy of ETE of MgR was carefully investigated. Two sterilized MgR (D = 0.7 mm, L = 9 mm) were directly placed in 12-well plates and co-cultured with the mouse osteoblastic cell line MC3T3-E1, and the mouse fibroblast cell line BALBc/3T3, for 1, 3, and 5 days, respectively, to verify its biocompatibility. We found that the MgR displayed good biocompatibility and even promoted the proliferation of both types of cells in short term (Fig. 2A and B). When the cells reached 100% confluence after several days, contact inhibition stabilized the number of living cells. Due to the high proliferation rate of BALBc/3T3 cells, a significant difference in the relative proliferation of BALBc/3T3 cells could only be observed on the 3rd day, instead of the 5th day (Fig. 2A and B). To verify the *in vitro* ETE of MgR on OS cells, two sterilized MgR (D = 0.7 mm, L = 9 mm) were directly added into the K7M2 OS cell line. Upon adjusting the electric field intensity of the AMF, the temperature in the culture dish reached to 42 °C, 47 °C and 52 °C, respectively. The pseudopodia of the cells disappeared, and the cells turned round after the treatment at 42 °C and 47 °C, while the cells treated at 52 °C became elongated and thin, indicating the great damage of ETE of MgR (Fig. S5). The methyl thiazolyl tetrazolium (MTT) assay revealed that more than half of the cells were dead after the treatment at 42 °C. With the increase in temperature, the proliferation of OS cells further decreased, and almost all the cells were killed at 52 °C by the ETE (Fig. 2C). To further determine the effect of heat alone, the cells were placed directly on a heating pad and heated to the specified temperature. The heat alone had similar effect on the cells as that of the ETE treatment (Fig. S6). The ETE heat induced by MgR played an important role in mediating cytotoxic effects in the K7M2 tumor cells. At the same time, the live and dead cells were co-labeled with the calcein acetoxymethyl ester (Calcein AM) and propidium iodide (PI) respectively (Fig. 2D), which indicated that only AMF or MgR alone did not induce cell death in the K7M2 cells, while the intensity of the red signal gradually enhanced with the ETE, indicated an increasing cell death. Interestingly, almost all the cells died under AMF after being incubated for 24 h, suggesting the induction of programmed cell death in the OS cells upon exposure to ETE (Fig. S7). Fluorescence activated cell sorting (FACS) analysis of the treated cells demonstrated that almost all the cells exposed to heat entered the apoptotic or necrotic process after being incubated for 8 h. With the rise of the treatment temperature induced by

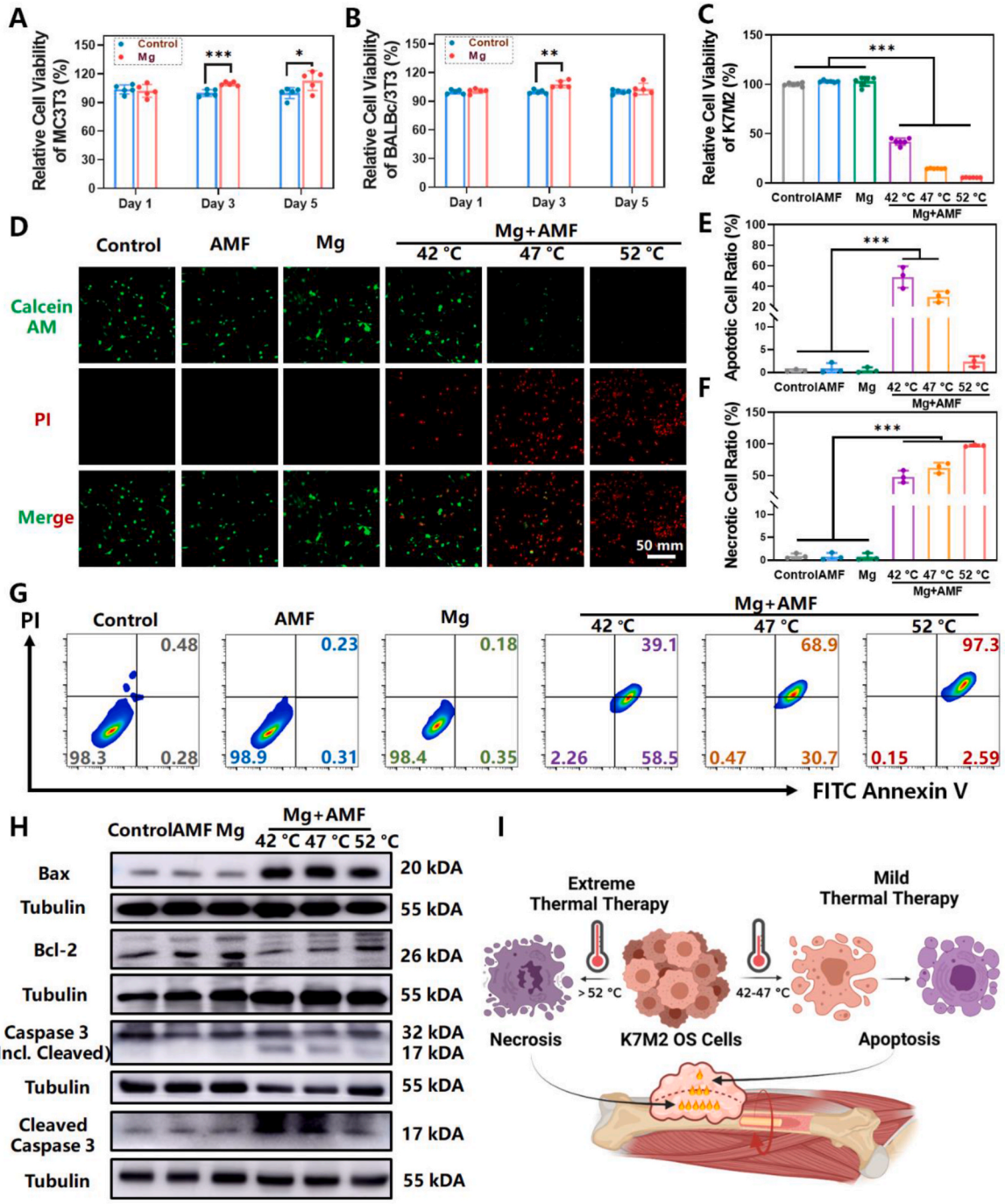

Fig. 2. ***In vitro*** **magnetic hyperthermia ablation of magnesium rod on OS. A.** Cell viability of MC3T3-E1 after exposure to MgR for long term (N = 5). **B.** Cell viability of BALBc/3T3 after exposure to MgR for long term (N = 5). **C.** Cell viability of K7M2 8 h after the ETE of MgR (N = 6). **D.** Live/Dead staining 8 h after the ETE of MgR. Quantity analysis of the flow cytometer on the K7M2 OS cells after the ETE of MgR (N = 3). **E.** Apoptotic; **F.** Necrotic. **G.** Representative flow cytometer data of Annexin V/PI. **H.** Western blotting of K7M2 OS cells 1 h after the ETE of MgR. **I.** Schematic illustration for the magnetic hyperthermia ablation of OS. The diameter and the length of MgR is 0.7 mm and 9 mm.

the ETE, the proportion of necrotic cells gradually increased, while that of the apoptotic cells gradually decreased (Fig. 2E–G). Finally, the apoptosis-related proteins in the K7M2 cells were detected. B-cell lymphoma 2 (Bcl-2) was found downregulated in K7M2 cells treated at 42 °C and 47 °C. While Bcl-2 associated X (Bax) was overexpressed in MHT groups compared with the control cells (Figs. S8A and B). Apoptosis was only induced when the ratio of Bax to Bcl-XL was maintained at a high ratio, meaning a high expression of Bax and low expression of Bcl-XL [26]. Bcl-XL is an important protein belonging to the Bcl-2 family [27]. Furthermore, the expression levels of Total and Cleaved Caspase 3, classic apoptosis markers, were detected. Cleaved Caspase 3 was overexpressed and the expression ratio of Cleaved and Total Caspase 3 was significantly increased in K7M2 cells treated at 42 °C and 47 °C (Figs. S8C and D). However, Caspase 3 was not activated in cells treated with 52 °C (Fig. 2H). All these results indicated that the relatively lower temperature (42 °C and 47 °C) treatment promoted apoptosis, different from that in relative higher temperature (52 °C, Fig. 2H). The heating effect was not uniform in the local ETE of MgR, and FACS could only analyze the single cells. Despite the results for the apoptosis assay measured by FACS was the highest in the severe MHT group, we still

speculated that the higher temperature treatment (52 °C) might trigger necrosis rather than apoptosis. Therefore, by adjusting the ETE of MgR, we expected to achieve a comprehensive therapeutic effect in OS by inducing necrosis triggered by severe MHT (>47 °C) and the apoptosis induced by the mild MHT (42–47 °C, Fig. 2I).

2.3. *In vivo* inhibitory effect of the EDT effect of MgR on OS

Inspired by the outstanding *in vitro* results of the ETE and the excellent biocompatibility of the MgR, we further evaluated the *in vivo* ETE of the MgR for the treatment of OS. First of all, the biocompatibility of MgR was assessed upon their long-term implantation in mice. No significant differences were found in the blood tests between the control and the implanted group. In addition, the local implantation of MgR did not affect the release of Mg in the serum (Figs. S9–10), which is consistent with the former studies [25,28]. More importantly, Mg does not have any side effects on peripheral organs (Fig. S11). Next, K7M2 OS cells were injected into the femoral bone marrow cavity of Balb/c mice. Two weeks after implantation, the sterile MgR (D = 0.7 mm, L = 9 mm) were implanted in the affected limbs of the tumor bearing mice, and the mice were subjected to treatment under an AMF on the next day (Fig. 3A). Due to cavity injection, OS was originated from the bone marrow cavity and the intramedullary implant was applied to achieve uniform heating for subsequent demonstration. It is well known that OS is a type of solid tumor initiated from bone invading outwards. Based on this, we maintained the epidermal temperature of the affected limbs at 42 °C for 10 min to obtain a comprehensive therapeutic effect against OS (Fig. 3B). Tumors in the control groups receiving AMF, and single MgR implantation, respectively, showed a steady tumor growth (Fig. 3C–G). After receiving MHT mediated by the MgR, the tumors showed obvious growth inhibition during the first week. However, the thigh circumference gradually increased on the second weekend before the obvious recurrence of murine OS in the third week (Fig. 3C–G). Histological analysis further displayed that the tumors in the control groups (single AMF and single MgR implantation) rapidly grew and obviously invaded all the soft tissues of the thigh. However, after MHT treatment, the tumor growth was remarkably inhibited (Fig. 3E), indicating that MHT played a protective role in OS treatment. During the MHT treatment, there were no systemic organ abnormalities or weight loss in the local MHT group (Figs. S12–13). Moreover, micro computed tomography (micro-CT) scanning displayed apparent osteoclasia in the femur in the control, AMF, and single MgR implantation groups, which was however much less in the local MHT group (Fig. S14).

Established by harvesting the secondary pulmonary metastatic lesions of the K7 OS cell line, the K7M2 OS cells have been well known for their highly invasive nature, with lung metastasis rates of over 90% in mice [29,30]. Therefore, we further evaluated lung metastasis in mice. Despite the good inhibitory effect of MHT, it could not completely prevent lung metastasis in the K7M2 tumor bearing murine, more specifically, the metastatic nodules were still found in the lung tissue sections after the ETE treatment. Quantity analysis of the pulmonary nodules demonstrated a significant suppression of metastases by MHT treatment compared with the other groups, which could probably be attributed to the reduction in the amount of blood vessels by MHT (Fig. 3H–I). The recurrence and metastasis observed in the MHT alone group was unsatisfactory, thus, it was worth exploring further strategies for the radical treatment of OS.

2.4. Immunogenic cell death and dendritic cells maturation of osteosarcoma cells caused by the eddy thermal effect of MgR

As a novel treatment, immunotherapy has been demonstrated to show reliable therapeutic effects on the inhibition of tumor growth and metastasis. However, the TME, consisting of a network of immune cells, promotes tumor proliferation and helps OS cells to escape from the immune system by hijacking critical physiological pathways [31]. Based on these, immunotherapy alone would be unable to reprogram the highly immunosuppressive TME in OS. Therefore, it is a promising strategy to enhance the efficacy of immunotherapy by inducing immunogenic cell death (ICD) in tumor cells. ICD results in the release of tumor-associated antigens (TAAs), tumor-specific antigens, risk-associated molecular patterns as well as pro-inflammatory

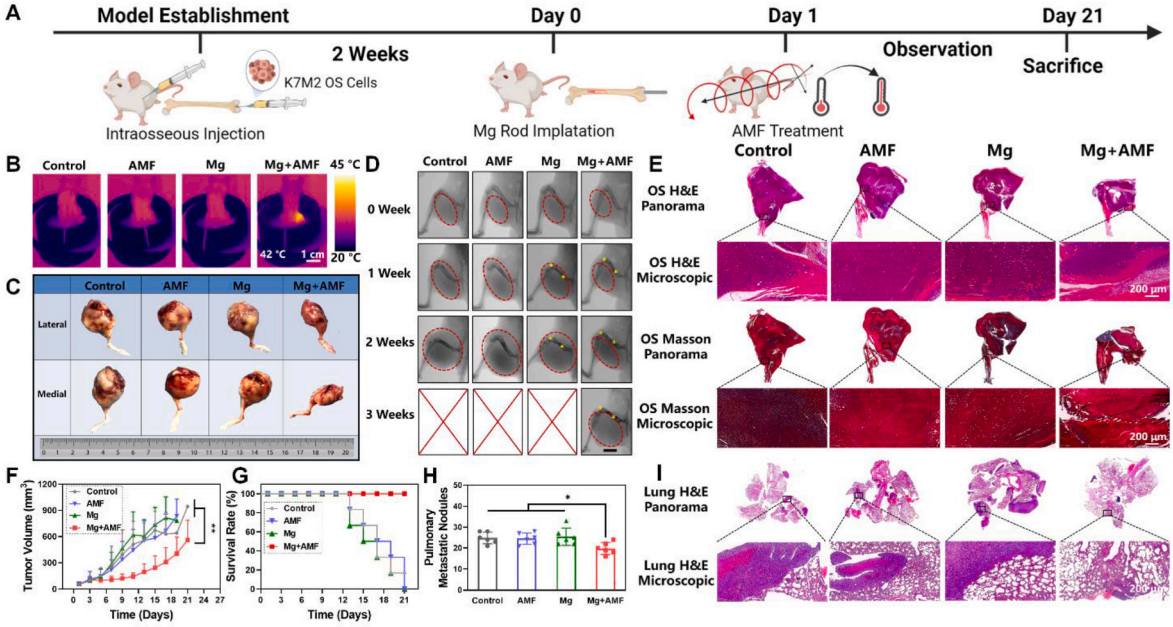

Fig. 3. ***In vivo*** **inhibitory effect of the eddy thermal effect of Mg on OS**. **A.** Schematic illustration for *in vivo* evaluation. **B.** Thermal pictures of mice implanted with MgR (D = 0.7 mm, L = 9 mm) under AMF. **C.** The general photographs of osteosarcoma harvested from mice. **D.** The X-ray images of mice after various treatments. Red dashed lines indicate the tumors. Yellow dots indicate the MgR implants.**E.** Representative H&E and Masson staining of osteosarcoma after the various treatments. **F.** The growth curve of osteosarcoma after the various treatments (N = 6). **G.** Survival rate of mice after the various treatments (N = 6). **H.** Pulmonary metastatic nodules of mice (N = 6). **I.** Representative H&E staining of lungs after the various treatments.

cytokines that trigger the adaptive immune cells to initiate an anti-tumor immune response [32]. Several studies have revealed the positive effect of hyperthermia therapy on inducing ICD in the tumor cells [33–35]. From the above results, it was found that the eddy thermal therapy mediated by MgR could cause apoptosis (mild thermal effect) and necrosis (severe thermal effect) in OS cells. Thus, the effect of MHT at 42 °C and 52 °C on inducing ICD in OS cells were investigated, respectively. Firstly, the changes in mitochondrial membrane potential (MMP) of OS cells after MHT were detected (Fig. 4A). JC-1 (CBIC2) exists as a polymer in the normal cells. However, when the mitochondrial membrane potential (MMP) is depolarized, JC-1 is released from inside as a monomer in the apoptotic cells, emitting green fluorescence.

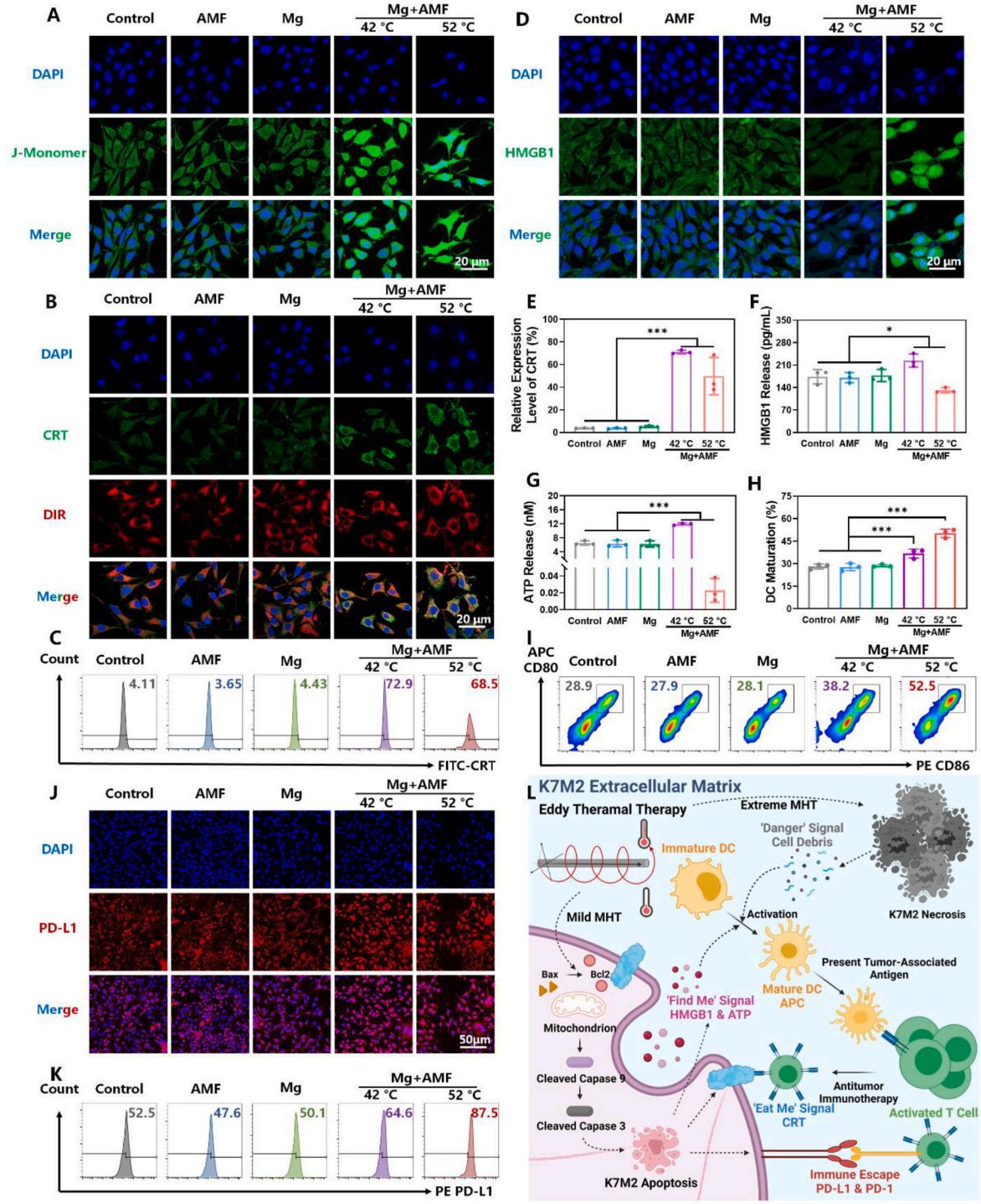

Fig. 4. The eddy thermal effect of Mg rods leads to immunogenic cell death and dendritic cells maturation of osteosarcoma cells. CLSM images of **A.** JC-1, **B.** CRT and **D.** HMGB1 of K7M2 after MHT. **C.** Representative flow cytometer data of CRT after the various treatments (N = 3). **E.** Quantity analysis of the flow cytometer on CRT after the various treatments (N = 3). **F.** ELISA kit for the detecting HMGB1 release of K7M2 after MHT (N = 3). **G.** ATP release of K7M2 after MHT (N = 3). **H.** Quantity analysis of the flow cytometer on DC maturation (N = 3, in the gate of $CD11c^{+}$). **I.** Representative flow cytometer data of DCs maturation after the various treatments. J. CLSM images of PD-L1 after MHT. K. Representative flow cytometer data of PD-L1 after the various treatments. L. Schematic illustration for the magnetic hyperthermia ablation leads to immunogenic cell death and dendritic cells maturation of osteosarcoma cells.

Both the mild MHT (42 °C) and severe MHT (52 °C) induced abnormal MMP. The monomer JC-1, was significantly increased in OS cells after MHT, further demonstrating the apoptotic effect of MHT. Additionally, mild MHT led to the disappearance of cell pseudopodia. On the other hand, the morphology of the OS cells became irregular after exposure to severe MHT, further suggesting the distinct death pathways triggered by mild versus severe MHT. Considering the intensities of green fluorescence and cell morphology, we demonstrated the abnormal MMP and apoptosis in K7M2 OS cells were caused by mild MHT.

Then, the expression of the 'eat me' signal calreticulin (CRT), was investigated. CRT rapidly translocates from the endoplasmic reticulum to the cell surface within a few hours after the initiation of ICD, as an 'eat me' signal, which is recognized by the phagocytes [36]. Both the confocal laser scanning microscope (CLSM) images and FACS analysis indicated that CRT translocation was caused by mild and extreme MHT. However, only a small number of single cells were collected in the severe MHT treated group, which meant that most of the cells were dead and disintegrated upon exposure to such high temperature (Fig. 4B, C and E). Afterwards, the release of the 'find me' signal, including adenosine triphosphate (ATP) and high mobility group box 1 (HMGB1), was detected as well. HMGB1 binds with TLR4 on immature dendritic cells (DCs) membrane to induce DCs maturation and presents antigen to activate the cytotoxic T lymphocytes (CTL) [37], while ATP recruits DCs and then activates the NLRP3 inflammasome to further eliminate the cancer cells [38]. As expected, the mild MHT mediated by MgR increased the release of the 'find me' signal, ATP and HMGB1, which led to the ICD of K7M2 OS cells (Fig. 4D, F and G). On contrary, the cells treated with severe MHT released much less ATP and HMGB1 than that of the control group (Fig. 4D, F and G). The release of HMGB1 involves nuclear membrane transfer and plasma membrane transfer. Confocal fluorescence images showed the significant decrease in the cytoplasmic expression of HMGB1 in the mild MHT group, indicating the release of HMGB1 (Fig. S15). On the other hand, a large amount of free cytoplasmic HMGB1 was found in the severe MHT group. Heating is a process from low temperature to high temperature and severe MHT comes from the mild MHT. We hypothesized that the ETE process could accelerate the transfer of HMGB1 to the nuclear membrane. However, severe MHT might lead to a quick cell death before the transfer of HMGB1 out of the membrane, resulting in lower levels of HMGB1 in the extracellular matrix in the severe MHT group. Furthermore, ATP is released in an autophagy-dependent manner, and the intense physical stimulation may cause a direct cell death instead of autophagy.

Finally, the effect of ETE on the maturation of bone marrow-derived dendritic cells (BMDCs) was explored. The supernatants of cells exposed to both mild and severe MHT treatment caused a high expression of CD80 and CD86 in BMDCs, indicating the maturation of BMDCs (Fig. 4H and I). Although mild MHT increased the expression of CRT and the release of HMGB1 along with ATP in K7M2 OS cells, the absolute value of the release concentration was much lower than that in the CT26 and other cancer cells [39]. Namely, K7M2 OS cells had relatively low immunogenicity. Thus, the effect of the supernatants from K7M2 OS cells treated with mild MHT on BMDCs maturation was limited to some extent. However, the cell supernatant from the severe MHT group greatly enhanced the maturation of the BMDCs. According to Matzinger's theory of danger signals, the cell debris disintegrated by non-apoptotic death (necrosis) is a dangerous signal that activates antigen-presenting cells and induces an immune response [40]. Therefore, we speculated that both the mild and severe MHT played crucial roles in the treatment of OS (Fig. 4L). Overall speaking, mild MHT leads to immunogenic death of tumor cells, releasing TAAs. While extreme MHT results in tumor cell necrosis and large amounts of cell debris release. Both ways could effectively stimulate DCs maturation for antigen presentation and immunotherapy. As a macroscopic metal, the uneven ETE of MgR enabled comprehensive MHT for mediating a variety of immune responses.

2.5. ETE of the MgR promotes the high expression of the immune checkpoint PD-L1

MHT enhanced the immunogenicity of tumor cells and the immune response *in vivo*, but it still could not cure tumors radically. Recently, the discovery of immune checkpoints has revealed the negative regulation on immune cells in the TME. Immune checkpoints and their ligands are frequently up-regulated in the TME, posing significant barriers for the induction of effective anti-tumor immune responses. Among the numerous immune checkpoints, programmed death 1 (PD-1) and programmed cell death-ligand 1 (PD-L1) have shown a strong correlation with the progression and metastasis of OS [41]. These two molecules bind to each other, producing the inhibitory signal that reduces the activity of immune cells, thus blocking the efficacy of immunotherapy against the tumor cells [42]. The infiltration of lymphocytes in tumors is usually accompanied by high PD-L1 expression. Despite the excellent cytotoxicity of the eddy thermal effect, it could have caused a high expression of PD-L1 in the OS TME. Clinical studies have revealed a high expression of PD-L1 in tumors after radiofrequency ablation or thermal vapour ablation [43,44]. While in animal tests, Huang et al. reported that mild photothermal therapy upregulated the expression of PD-L1 in the tumor cells [45]. Previous studies have reported that PD-L1 was expressed at a high level in K7M2 OS cells [46]. Recent studies have also shown that mild cytotoxicity may lead to a higher expression of PD-L1 in K7M2 cells, resulting in drug resistance, which further elucidates the necessity of ICB to enhance the efficacy of immunotherapy [47]. Thus, whether the ETE caused by MgR would lead to a high expression of PD-L1 in K7M2 was further analyzed.

Confocal fluorescence images showed a strong red fluorescence intensity in the MHT groups, indicating a high expression of PD-L1 after both mild and severe MHT exposure (Fig. 4J and S16A). Flow cytometry results further confirmed the above results (Fig. 4K and S16B). In spite of the high expression level of PD-L1 in K7M2 cells, the thermal effect further upregulated the expression of PD-L1 in these cells. PD-L1 interrupts the communication between the tumor-infiltrating lymphocytes (TILs) and cancer cells, resulting in the failure of single MHT in OS (Fig. 4L).

2.6. Combination of the ETE of MgR with immunotherapy

Encouraged by the ICD, BMDCs maturation and high expression of PD-L1 caused by the ETE of MgR, the immune checkpoint, PD-L1, was further blocked and combined with MHT to treat OS, wherein, MHT might improve the infiltration of immune cells into the tumor, before the enhanced local immune effect mediated by PD-L1 targeted antibodies. Firstly, K7M2 OS cells were injected into the femoral bone marrow cavity of the Balb/c mice. After two weeks of the tumor model establishment, sterile MgR (D = 0.7 mm, L = 9 mm) were implanted into the femur of the mice, then MHT was performed on the next day (Fig. 5A). We kept the epidermal temperature of the mice at 42 °C to obtain a comprehensive OS treatment. On the second, fourth and sixth days after MHT, anti-PD-L1 (200 μg/mouse) was intraperitoneally injected into the mice (Fig. 5A–B). Both the mild and severe MHT exposure promoted the antigen-presenting efficacy of the DCs. On the one hand, the inner temperature was higher than that of the outside, leading to the necrosis of the internal tumor. The inner tumor disintegrated into debris acted as an immune adjuvant to enhance the immune response. On the other hand, the external tumor tissue was treated with mild MHT to induce apoptosis and ICD for further immunotherapy.

Among the various treatments, MHT alone and the anti-PD-L1 alone showed a certain inhibitory effect on the development of OS (Fig. 5C–D). But the tumors kept growing, indicating a tendency for recurrence. The PD-L1 antibody or MHT alone were unable to fully suppress OS progression. Surprisingly, the tumor size of mice was remarkably inhibited after exposure to the combination of MHT and anti-PD-L1 immunotherapy. Despite the recurrence tendency at the end of the three-week

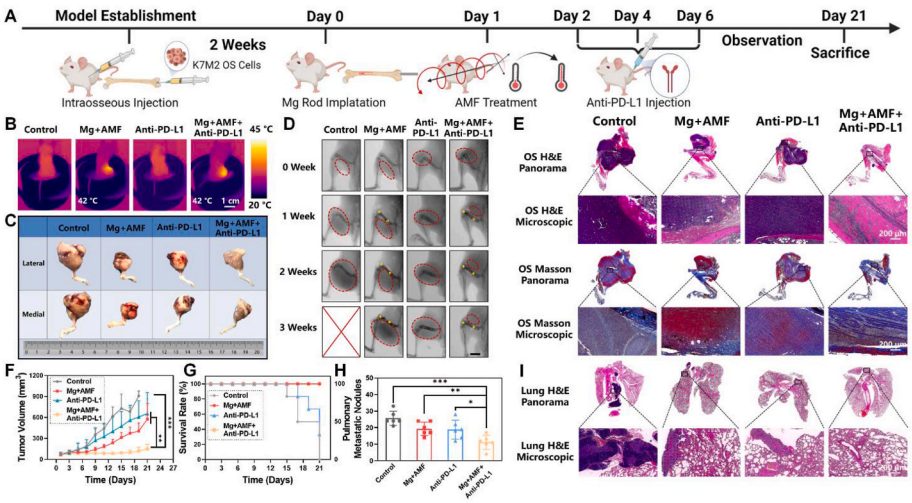

Fig. 5. ***In vivo*** **radical treatment of osteosarcoma by the eddy thermal effect of Mg rod combined with immune checkpoint blocking. A.** Schematic illustration for the *in vivo* evaluation. **B.** Thermal pictures of mice implanted with MgR (D = 0.7 mm, L = 9 mm) under AMF. **C.** The general photographs of osteosarcoma harvested from mice. **D.** The X-ray images of mice after the various treatments. Red dashed lines indicate the tumors. Yellow dots indicate the MgR implants. **E.** Representative H&E and Masson staining of osteosarcoma after the various treatments. **F.** The growth curve of osteosarcoma after the various treatments (N = 6). **G.** Survival rate of mice after the various treatments (N = 6). **H.** Pulmonary metastatic nodules of mice (N = 6). **I.** Representative H&E staining of lungs after the various treatments.

observation, the tumor progression was significantly suppressed, which showed a significant therapeutic advantage of the combination strategy in comparison with MHT or anti-PD-L1 treatment alone (Fig. 5C–G). The findings from the histological analysis were also consistent with the above results. The tumor volume in the combination therapy group was smaller compared with the other groups. However, the dying tumor tissue after MHT was still present in the periphery of the femur, and the tumor-like tissue could also be observed in the outermost subcutaneous area, potentially because the uneven MHT mediated by the ETE could not induce apoptosis and ICD in all sites around the tumor (Fig. 5E). Compared with the combination therapy, monotherapy with a MHT or anti-PD-L1 antibody caused an irreversible recurrence in the 3rd week. Commendably, the number of lung metastases significantly reduced in mice treated with the combination therapy. More importantly, the local MHT mediated by MgR exerted a distal effect to achieve systemic OS treatment (Fig. 5H–I). Moreover, the combination therapy did not cause systemic organ abnormalities, weight loss or bone defect in the mice (Figs. S17–19). All the above results demonstrated the excellent therapeutic efficacy of MHT combined with immunotherapy in OS.

2.7. The ETE of MgR modulates the TME and enhances immunotherapy efficacy

Next, a deeper exploration of the mechanism of the combination therapy was investigated in OS. The same procedure of MHT combined with anti-PD-L1 antibody was applied (Fig. 6A). On the seventh day, the immune microenvironment in the mice bearing OS tumors after the various treatments was evaluated. The results proved the definite influence of the ETE of MgR in modulating TME and enhancing immunotherapy. DCs are one of the important antigen-presenting cells, and the maturation of DCs in the proximal inguinal lymph nodes was dramatically enhanced after MHT, indicating a strong induction of antigen presentation leading to the activation of the immune system and cellular immunotherapy [48] (Fig. 6B and G). T-lymphocytes and tumor-associated macrophages (TAMs) constitute the majority of the immune landscape of OS. There are several subtypes of T cells that have totally different function in the tumors. Among the various subtypes, multiple studies have highlighted a strong correlation between cytotoxic T lymphocytes (CTLs, CD8 positive TILs) and better prognosis of cancer patients [49,50]. Enhancing the infiltration of CTLs into the OS TME has been reported to improve the therapeutic efficacy of cancer immunotherapy [51,52]. Inspiringly, the ETE treatment could boost CTLs infiltration in OS, with an average rate around 30% (Fig. 6C and H), while it was only about 20% in the control group and the anti-PD-L1 antibody monotherapy group. Owing to MHT, the combination therapy also reached over 35% CTLs infiltration rate. The thermal effect caused by ETE had a positive effect on CTLs infiltration, which was consistent with the findings from former studies [44,45]. The proliferation and functions of CTLs were further evaluated. Proliferation of CTLs is a prerequisite for anti-cancer immune activity. Poggio et al. have revealed the inhibiting effect of PD-L1 on CTLs [53]. Luckily, ETE does not affect the proliferation of CTLs. While anti-PD-L1 therapy and the combinatory therapy significantly enhanced the ratio of Ki-67 positive CTLs up to 30% (Fig. 6D and I). Granzyme B, the most abundant serine protease in CTLs, plays a basic role in eliminating harmful target cells (tumor cells et al.) [54]. Our results have well demonstrate the positive effect of both ETE and anti-PD-L1 therapy on elevating the expression of Granzyme B in CTLs. Notably, the combinatory therapy could further improve the function of CTLs in tumor (Fig. 6E and J). The inflammation caused by ETE resulted in the high expression of interferon-γ (IFNγ) in CTLs, upregulating antigen presentation of DCs [48] (Fig. 6F and K). Overall speaking, ETE improves CTLs function and does not affect the proliferation. The immunotherapy could further enhance the proliferation of CTLs and make up for the weakness of ETE. Interestingly, the TAMs showed increasing M1 polarization and decreasing M2 polarization in OS after MHT treatment (Fig. 7A, B, E and F). Considering the polarization, TAMs might have different effects on the fate of tumors. In detail, TAMs with M1-like characteristics have the potential to kill tumor cells and enhance the immune response, the M2-like TAMs exhibit an immunosuppressive phenotype in most tumors, promoting the progression, invasion, and metastasis of tumors [55]. Moreover, the expression of the key inflammatory factors, interleukin-1β (IL-1β) and tumor necrosis factor-α (TNF-α), were significantly elevated in the TME after MHT (Fig. 7I and J). A large number of inflammatory factors are conducive to immune cell infiltration and immune activation. Our work revealed the remodeling of the immune microenvironment from anti-inflammatory to pro-inflammatory in OS, which suppressed the immune-suppressive environment in OS.

Based on the *in vitro* results, the expression of PD-L1 was evaluated *in vivo*. After MHT treatment, there was a significant increase in the expression of PD-L1 both on the surface of the tumor cells and the TILs. The activation of immune checkpoints has a strong impact on suppressing the anti-tumor immune response. For immunotherapy alone, anti-PD-L1 therapy caused a decrease in the expression of PD-L1 in both tumor cells and TILs. However, due to the low infiltration rate of immune cells in the TME, immunotherapy efficacy was reduced by the limited number of effective effector cells. Though there was no significant difference between the combinatory therapy group and the control group regarding the expression of PD-L1 *in vivo*, anti-PD-L1 therapy reversed the high expression caused by MHT (Fig. 7C, D, G and H).

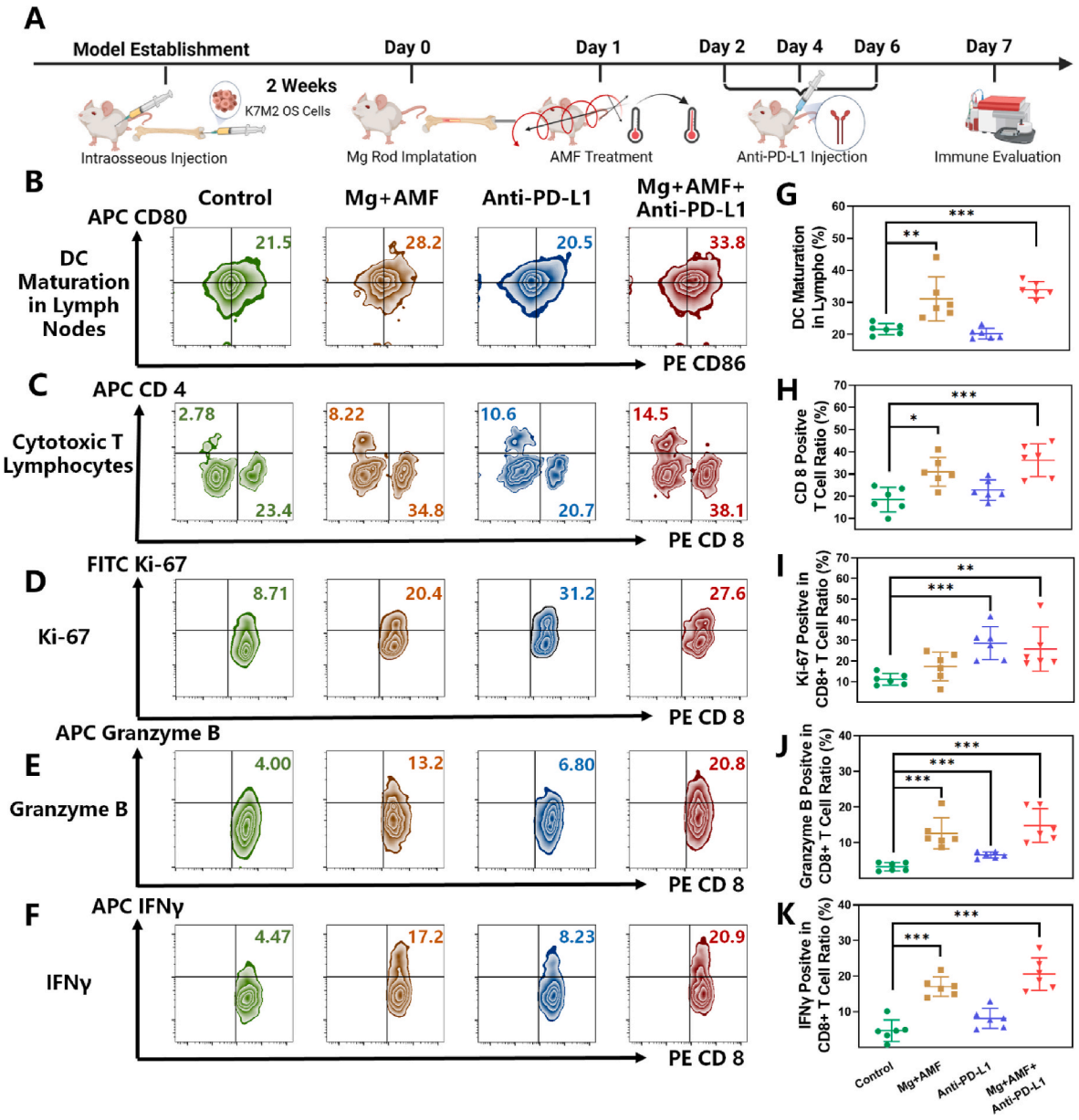

Fig. 6. The eddy thermal therapy of Mg rods improves DCs maturation and T cells function. A. Schematic illustration for *in vivo* evaluation. Representative flow cytometer data of **B.** DCs maturation in lymph nodes (in the gate of $CD11c^+$), **C.** T-cell (in the gate of $CD3^+$ and $CD45^+$), **D.** Ki-67, **E.** Granzyme B and **F.** IFNγ in $CD8^+$ T cells (in the gate of $CD3^+$, $CD45^+$ and $CD8^+$). Quantity analysis of the flow cytometer (N = 6) on **G.** DCs maturation in lymph nodes, **H.** $CD8^+$ T-cell in tumors, **I.** Ki-67, **J.** Granzyme B and **K.** IFNγ in $CD8^+$ T cells.

Sufficient numbers of TILs and the reconstruction of the communication between the tumor cells and the TILs has rendered immunotherapy a strong therapeutic potential for treating OS.

The results from histological analyses were also consistent with the immunoassay results. TUNEL staining showed the strong positive signal in OS tissue treated with MHT, indicating the clear tumor apoptosis induced by MHT. The expression of Ki-67 in the cell nucleus was significantly decreased in the MHT and the combination therapy groups, suggesting the inhibition of the proliferation of OS cells. Meanwhile, the expression of the characteristic proteins associated with the M1 phenotype, including CD86 and CD68, further verified the M1 polarization of the TAMs (Fig. 7K and S21). Regarding PD-L1 expression, immunofluorescence staining showed similar results as above (Fig. 7L and S22). Therefore, all of the above results demonstrated that ETE of MgR inside the tumor activated the immune system and further elicited robust immune responses to inhibit OS upon combination with anti-PD-L1 checkpoint blockade therapy (Fig. 7M).

2.8. Mg rods enhance osteogenic activity

Mg ions have the strong ability to promote bone regeneration by enhancing matrix mineralization and increasing the expression of osteogenesis related genes and proteins [56,57]. The *in vitro* osteogenic ability of MgR was firstly investigated on the mouse osteoblastic cell line MC3T3-E1. MgR extract was obtained by incubating Mg rod (D = 0.7 mm, L = 9 mm, 1 rod/mL) in high-glucose Dulbecco's modified Eagle's medium at 37 °C for 3 days. Alkaline phosphatase staining and activity measurement showed a high level of alkaline phosphatase expression and activity upon treatment with 5 mM Mg^{2+} and MgR extract (Fig. 8A and B). Alizarine red staining also showed more calcium nodules in the Mg^{2+} and MgR extract treated groups after long-term induction (Fig. 8C and D). Subsequently, the expression of osteogenesis-related genes in

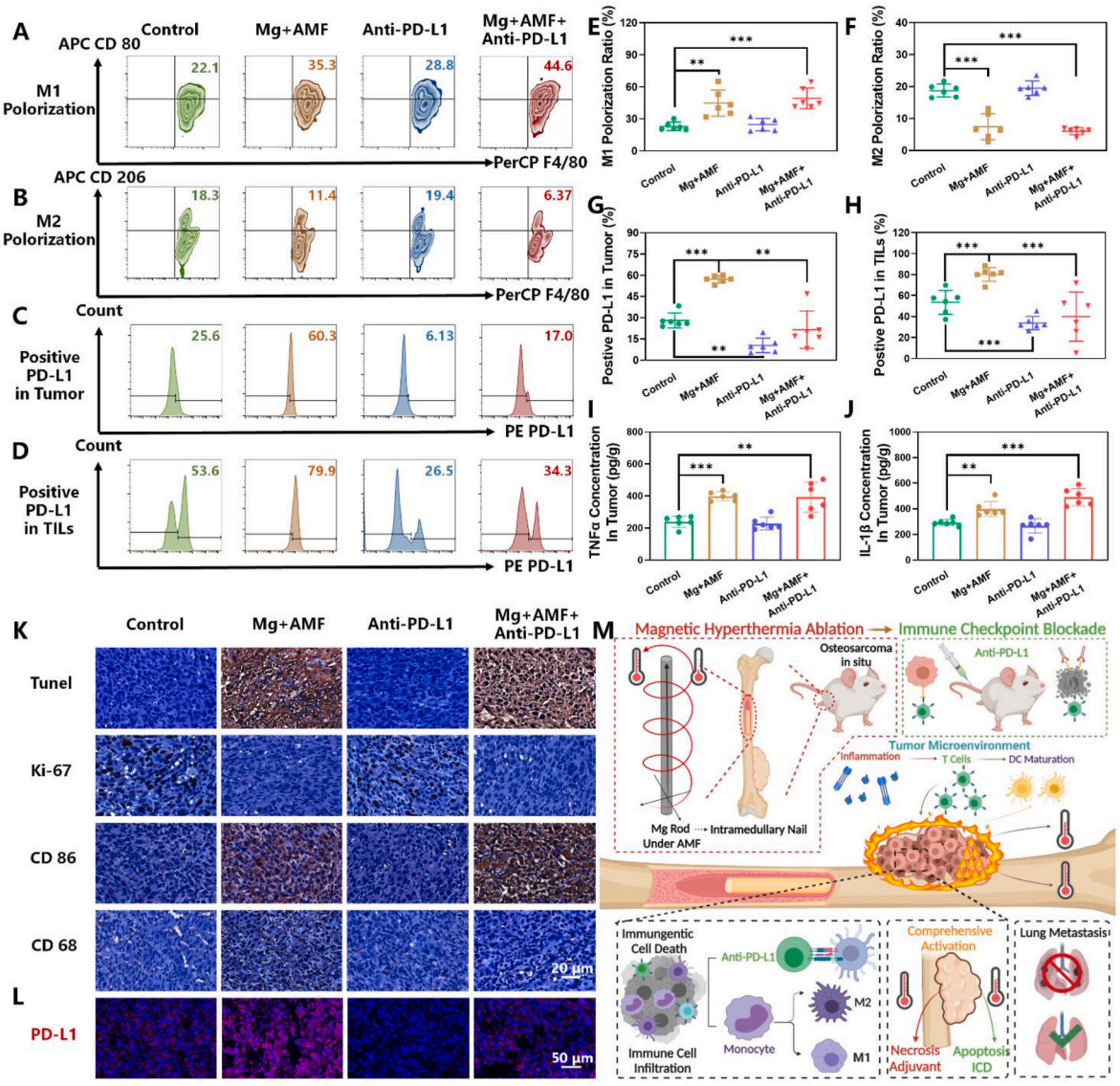

Fig. 7. The eddy thermal therapy of Mg rods modulates TME and enhanced immunotherapy. Representative flow cytometer data of **A.** M1 Polorization, **B.** M2 Polorization in tumors (in the gate of $CD11b^+$ and $CD45^+$) and **C.** PD-L1 positive in tumor (in the gate of $CD45^-$). **D.** PD-L1 positive in tumor infiltrating lymphocytes (in the gate of $CD45^+$). Quantity analysis of the flow cytometer (N = 6) on **E.** M1 Polorization, **F.** M2 Polorization in tumors, **G.** PD-L1 ratio on tumor, **H.** PD-L1 ratio on TILs, and ELISA kit for detecting **I.** TNF-α and **J.** IL-1β in tumor after the various treatments (N = 6). **K.** Histological analysis of tumors after the various treatments. **L.** Histological immunofluorescence of PD-L1 of tumors after the various treatments. **M.** Schematic illustration of the comprehensive radical therapy of the ETE of MgR.

MC3T3-E1 cells was further analyzed after osteogenic induction, by quantitive real-time polymerase chain reaction (qRT-PCR). The expression of early (alkaline phosphatase, ALP), intermediate (collagen I), and late (osteocalcin, OCN) osteogenesis-related genes were all prominently elevated (Fig. 8F). Compared with the MgR extract group, the Mg^{2+} treated cells featured a more stable osteogenic performance, which might be caused by the difference in the degradation rate of MgR. Finally, the mechanism of osteogenesis was briefly studied by western blotting (WB) analysis. The expression of Wnt and β-catenin in MC3T3-E1 cells treated with 5 mM Mg^{2+} and MgR extract were effectively promoted. Furthermore, β-catenin displayed strong nuclear translocation after Mg^{2+} treatment, suggesting the activation of canonical Wnt signaling pathway by Mg^{2+} and MgR. (Fig. 8E and G, S23 and S24). Along with the formation of $Mg(OH)_2$, the degradation of MgR led to an alkaline environment (pH ~8.0) [57,58]. The osteogenic differentiation and mineralization process has not been reported to be significantly influenced by the moderate external alkaline pH but was dramatically inhibited at higher pH (>7.9) [59]. Consistent with the previous studies, the treatment at higher pH = 8.0 showed no obvious osteogenic effect, further indicating the important role of the released Mg^{2+} in promoting osteogenesis. The above results laid sufficient theoretical foundation for MgR in tackling critical bone defects.

Inspired by the above positive results, the *in vivo* osteogenic effect of MgR on osteogenesis was evaluated using a murine femur fracture model [60]. Stainless steel needles (D = 0.7 mm, L = 9 mm) and MgR (D = 0.7 mm, L = 9 mm) were implanted as intramedullary nails, respectively (Fig. S25). After six-week observation, Micro-CT analysis displayed a large number of calluses at the fracture site in the control group, while the surface of the fracture site was smooth and flat in the MgR group. The bone regeneration process in the MgR group was faster than that in the control group (Fig. 7H). Micro-CT quantity analysis also indicated a significantly higher level of the percent bone volume and bone surface density in the MgR group, further suggesting the excellent osteogenesis inducing ability of MgR (Fig. 7I). Compared with the

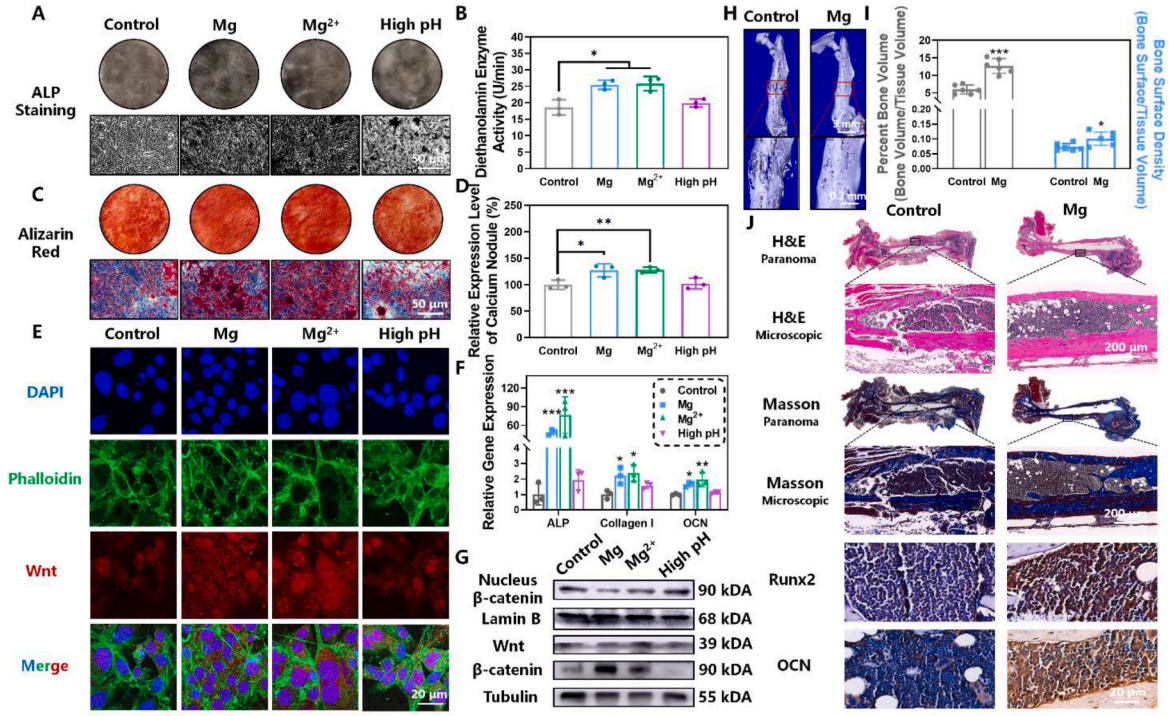

Fig. 8. Magnesium rods enhance osteogenic activity. **A.** ALP staining and **B.** activity of MC3T3-E1 after 7 days of osteogenesis induction (N = 3). **C.** Alizarin red staining of MC3T3-E1 after 14 days of osteogenesis differentiation. **D.** Quantity analysis of alizarin red staining (N = 3). **E.** Confocal fluorescence images of WNT in MC3T3-E1 after 7 days of osteogenesis induction. **F.** Gene expression of ALP, collagen I, and OCN after various treatments (N = 3). **G.** Western blotting analysis of WNT/β-catenin pathway in MC3T3-E1 after 7 days of osteogenesis differentiation. **H.** Representative Micro-CT reconstruction images. **I.** Quantity analysis of Micro-CT (N = 6). **J.** Histological analysis of the fractured femur after the different treatments.

control groups, the histological staining as well as the Masson staining showed that the fracture line implantation had basically disappeared in the MgR group (Fig. 7J). Moreover, there was a large amount of collagen at the fracture site and obvious bone regeneration in the MgR group. Decalcification before section degrades the implant and only an empty bone marrow cavity could be found. Lastly, the immunohistochemical staining further indicated that both Runx2 and OCN were highly expressed in the MgR implantation group (Fig. S26). All these results strongly revealed the promising effect of MgR on bone regeneration and repair.

3. Conclusion

In summary, the ETE of biodegradable magnesium rods had a definite therapeutic effect on osteosarcoma. Our work has revealed the outstanding tumoricidal effects of eddy thermal therapy mediated by magnesium rods on osteosarcoma cells *in vitro*. Despite the limited *in vivo* therapeutic efficacy of the magnetic thermotherapy alone, the ETE of magnesium rods comprehensively activated the immune response, providing a theoretical basis for the radical treatment of OS. Combined with ICB therapy, we obtained excellent therapeutic efficacy against OS, and further analyses demonstrated that the local MHT mediated by the Mg rods increased T cell infiltration and M1 polarization of macrophages. Additionally, the Mg rods were also found to regenerate large bone defects after osteosarcoma.

Simple but effective, the ETE of biodegradable Mg rods offers several advantages and potential application in clinical OS therapy. Firstly, mass-produced Mg rods have a relatively ideal stability and efficiency compared with other thermo-magnetic agents. Secondly, the outstanding ability of Mg rods to promote osteogenesis and their high biocompatibility makes them optimal multifunctional agents in orthopedic applications. Notably, the eddy current thermal effect of macro metallic materials effectively regulates and remodels the TME. The current work demonstrates the feasibility to combine MHT mediated by macroscopic materials with immunotherapy for treating OS. Uneven heating, formerly considered to be the disadvantage of local ETE, has been verified as the key to comprehensive immunologic activation in OS. The result from the current study provide inspiration for further studies exploring the combination of MHT and immunotherapy for the radically treatment of OS.

Owing to the excellent heating performance of Mg, it is tempting to control the temperature in this process. But in fact, the location and the temperature of MHT can be effectively controlled by adjusting the size and the location of the Mg rods implant. In the clinical practice, the tumors are precisely located by contrast enhancement CT scan and MRI. By implanting the Mg rods of corresponding size into the tumor or at the excised tumor site under CT navigation, MHT combined with ICB, could not only effectively destroy the tumors from deep inside, but also prevent further metastatic spread. Moreover, the excellent osteogenic potential of the Mg rods provides a theoretical basis for the prevention of cancer-induced osteoporosis. Most importantly, Mg rods are simple and easy to be acquired, which further supports their clinical application (Scheme 1). However, the final translation of the technology is still challenging. Meanwhile, surface modification or shape optimization of MgR is necessary to strengthen the integration at bone and tumor site. On the other hand, a better surgical implantation technique is urgent to be explored to avoid metastasis as much as possible during the process of tumor excision or intratumoral implantation. Overall, OS could be treated by minimally invasive implantation of tiny Mg rods in the future. Upon further combination with immunotherapy, Mg rods-based MHT offers a new opportunity for treating OS and other solid tumors.

Author contributions

L. Cheng, H. Yang, and J. Zou conceived and designed the study, analyzed the data, and provided funding. J. Ge, N. Yang and Y. Yang

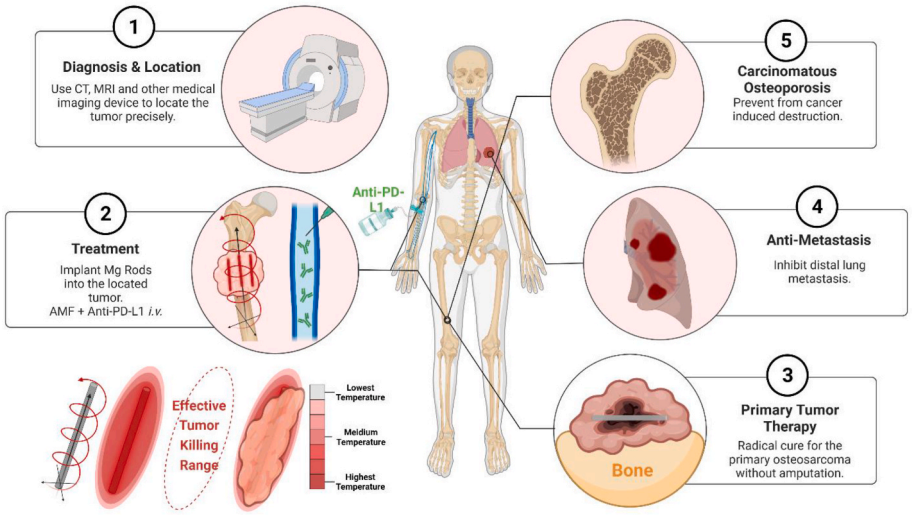

Scheme 1. Schematic illustration of the clinical application of the MHT and immunotherapy combinatory treatment for OS. By implanting the Mg rods with the corresponding size into the tumor under imaging navigation, MHT combined with immune checkpoint blockade can effectively destroy the tumor from deep inside and prevent from further metastasis. The excellent osteogenic property of Mg rods may further prevent cancer-induced OS.

carried out characterization of the MgR, both *in vitro* and *in vivo* evaluation and data analysis. H. Yu, Y. Wang, T. Wang and Y. Teng carried out *in vivo* OS model establishment, medical imaging acquirement and samples collection. X. Yang, S. Cheng, Y. Wang and Z. Han carried out immunological analysis. All authors wrote and approve the publication of the manuscript.

Ethics committee

(The First Affiliated Hospital of Soochow University) has approved the animal experiments.

Declaration of competing interest

The authors declare that they have no known competing financial interests or personal relationships that could have appeared to influence the work reported in this paper.

Acknowledgements

This article was partially supported by the National Natural Science Foundation of China (U20A20254, 52072253, 82172506, 82030068), Collaborative Innovation Center of Suzhou Nano Science and Technology, the 111 Project, Joint International Research Laboratory of Carbon-Based Functional Materials and Devices, a Jiangsu Social Development Project (BE2019658)., a Jiangsu Natural Science Fund for Distinguished Young Scholars (BK20211544), and Suzhou Key Laboratory of Nanotechnology and Biomedicine. L. Cheng was supported by the Tang Scholarship of Soochow University. We thank Li Wang, Haoran Liu, Lin Zhang, Huali Lei, Guangqiang Li, Xiang Gao, Linfu Chen, Muchao Chen, Liting Zhou and Yanglin Wu for discussions and modelling methods, Cenhao Wu and Lin Liu for animal experiments assistance, Zhuorun Song for X-Ray analysis, Yu Zhang, Jiewei Yin and Kang Wu for Micro-CT analysis. The authors would like to thank all the reviewers who participated in the review, MJEditor (www.mjeditor.com) for providing English editing services during the preparation of this manuscript, and the website of app.Biorender.com for the assistance in creating the illustration figures.

Appendix A. Supplementary data

Supplementary data to this article can be found online at https://doi.org/10.1016/j.bioactmat.2023.01.008.

References

[1] R.A. Durfee, M. Mohammed, H.H. Luu, Review of osteosarcoma and current management, Rheumatology and therapy 3 (2) (2016) 221–243.
[2] C. Meazza, P. Scanagatta, Metastatic osteosarcoma: a challenging multidisciplinary treatment, Expet Rev. Anticancer Ther. 16 (5) (2016) 543–556.
[3] S.S. Bielack, S. Hecker-Nolting, C. Blattmann, L. Kager, Advances in the management of osteosarcoma F1000Research (2016) 5.
[4] B.A. Lindsey, J.E. Markel, E.S. Kleinerman, Osteosarcoma overview, Rheumatology and therapy 4 (1) (2017) 25–43.
[5] B. Yang, J. Yin, Y. Chen, S. Pan, H. Yao, Y. Gao, J. Shi, 2D-black-phosphorus-reinforced 3D-printed scaffolds: a stepwise countermeasure for osteosarcoma, Adv. Mater. 30 (10) (2018), 1705611.
[6] C.S.o.C.O. (Csco, in: J. Hao (Ed.), Guidelines of Chinese Society of Clinical Oncology (CSCO) on Conventional Osteosarcoma, People's Medical Publishing House, China, 2020.
[7] M.J. Berger, D.S. Ettinger, J. Aston, S. Barbour, J. Bergsbaken, P.J. Bierman, D. Brandt, D.E. Dolan, G. Ellis, E.J. Kim, S. Kirkegaard, D.D. Kloth, R. Lagman, D. Lim, C. Loprinzi, C.X. Ma, V. Maurer, L.B. Michaud, L.M. Nabell, K. Noonan, E. Roeland, H.S. Rugo, L.S. Schwartzberg, B. Scullion, J. Timoney, B. Todaro, S. G. Urba, D.A. Shead, M. Hughes, NCCN guidelines insights: antiemesis, version 2.2017, J. Natl. Compr. Cancer Netw. : J. Natl. Compr. Cancer Netw. 15 (7) (2017) 883–893.
[8] M. Xu, Z. Wang, X.C. Yu, J.H. Lin, Y.C. Hu, Guideline for limb-salvage treatment of osteosarcoma, Orthop. Surg. 12 (4) (2020) 1021–1029.
[9] Z. Hedayatnasab, F. Abnisa, W.M.A.W. Daud, Review on magnetic nanoparticles for magnetic nanofluid hyperthermia application, Mater. Des. 123 (2017) 174–196.
[10] E.A. Périgo, G. Hemery, O. Sandre, D. Ortega, E. Garaio, F. Plazaola, F.J. Teran, Fundamentals and advances in magnetic hyperthermia, Appl. Phys. Rev. 2 (4) (2015), 041302.
[11] F. Gong, L. Cheng, N. Yang, Q. Jin, L. Tian, M. Wang, Y. Li, Z. Liu, Bimetallic oxide MnMoOX nanorods for in vivo photoacoustic imaging of GSH and tumor-specific photothermal therapy, Nano Lett. 18 (9) (2018) 6037–6044.
[12] Y.-s. Kim, W.J. Lee, H. Rhim, H.K. Lim, D. Choi, J.Y. Lee, The minimal ablative margin of radiofrequency ablation of hepatocellular carcinoma (> 2 and< 5 cm) needed to prevent local tumor progression: 3D Quantity assessment using CT image fusion, Am. J. Roentgenol. 195 (3) (2010) 758–765.
[13] J. Pan, Y. Xu, Q. Wu, P. Hu, J. Shi, Mild magnetic hyperthermia-activated innate immunity for liver cancer therapy, J. Am. Chem. Soc. 143 (21) (2021) 8116–8128.
[14] H. Gavilán, S.K. Avugadda, T. Fernández-Cabada, N. Soni, M. Cassani, B.T. Mai, R. Chantrell, T. Pellegrino, Magnetic Nanoparticles and Clusters for Magnetic Hyperthermia: Optimizing Their Heat Performance and Developing Combinatorial Therapies to Tackle Cancer, Chemical Society Reviews, 2021.
[15] C. Bean, R. DeBlois, L. Nesbitt, Eddy-current method for measuring the resistivity of metals, J. Appl. Phys. 30 (12) (1959) 1976–1980.
[16] C. Zhang, T.H. Wen, K.A. Razak, J. Lin, C. Xu, C. Seo, E. Villafana, H. Jimenez, H. Liu, Magnesium-based biodegradable microelectrodes for neural recording, Mater. Sci. Eng. C 110 (2020), 110614.
[17] S. Kamrani, C. Fleck, Biodegradable magnesium alloys as temporary orthopaedic implants: a review, Biometals 32 (2) (2019) 185–193.

[18] G.S. Feng, K.L. Hanley, Y. Liang, X. Lin, Improving the efficacy of liver cancer immunotherapy: the power of combined preclinical and clinical studies, Hepatology 73 (2021) 104–114.
[19] J. Fu, I.-J. Malm, D.K. Kadayakkara, H. Levitsky, D. Pardoll, Y.J. Kim, Preclinical evidence that PD1 blockade cooperates with cancer vaccine TEGVAX to elicit regression of established tumors, Cancer Res. 74 (15) (2014) 4042–4052.
[20] M.F. Wedekind, L.M. Wagner, T.P. Cripe, Immunotherapy for osteosarcoma: where do we go from here? Pediatr. Blood Cancer 65 (9) (2018), e27227.
[21] Y.T. Sundara, M. Kostine, A.H. Cleven, J.V. Bovée, M.W. Schilham, A.-M. Cleton-Jansen, Increased PD-L1 and T-cell infiltration in the presence of HLA class I expression in metastatic high-grade osteosarcoma: a rationale for T-cell-based immunotherapy, Cancer Immunology, Immunotherapy 66 (1) (2017) 119–128.
[22] C. Song, H. Phuengkham, Y.S. Kim, I. Lee, I.W. Shin, H.S. Shin, S.M. Jin, S.H. Um, H. Lee, K.S. Hong, Syringeable immunotherapeutic nanogel reshapes tumor microenvironment and prevents tumor metastasis and recurrence, Nat. Commun. 10 (1) (2019) 1–15.
[23] M.F. Heymann, K. Schiavone, D. Heymann, Bone sarcomas in the immunotherapy era, Br. J. Pharmacol. 178 (9) (2021) 1955–1972.
[24] J. Rytlewski, M.M. Milhem, V. Monga, Turning 'Cold'tumors 'Hot': immunotherapies in sarcoma, Ann. Transl. Med. 9 (12) (2021).
[25] J. Draxler, E. Martinelli, A.M. Weinberg, A. Zitek, J. Irrgeher, M. Meischel, S. E. Stanzl-Tschegg, B. Mingler, T. Prohaska, The potential of isotopically enriched magnesium to study bone implant degradation in vivo, Acta Biomater. 51 (2017) 526–536.
[26] N. Shinoura, Y. Yoshida, A. Asai, T. Kirino, H. Hamada, Relative level of expression of Bax and Bcl-X L determines the cellular fate of apoptosis/necrosis induced by the overexpression of Bax, Oncogene 18 (41) (1999) 5703–5713.
[27] M. Vogler, H.A. Hamali, X.-M. Sun, E.T. Bampton, D. Dinsdale, R.T. Snowden, M. J. Dyer, A.H. Goodall, G.M. Cohen, BCL2/BCL-XL inhibition induces apoptosis, disrupts cellular calcium homeostasis, and prevents platelet activation, Blood, The Journal of the American Society of Hematology 117 (26) (2011) 7145–7154.
[28] D. Zhao, T. Wang, K. Nahan, X. Guo, Z. Zhang, Z. Dong, S. Chen, D.-T. Chou, D. Hong, P.N. Kumta, W.R. Heineman, In vivo characterization of magnesium alloy biodegradation using electrochemical H2 monitoring, ICP-MS, and XPS, Acta Biomater. 50 (2017) 556–565.
[29] C. Khanna, J. Prehn, C. Yeung, J. Caylor, M. Tsokos, L. Helman, An orthotopic model of murine osteosarcoma with clonally related variants differing in pulmonary metastatic potential, Clin. Exp. Metastasis 18 (3) (2000) 261–271.
[30] B.T. Grisez, J.J. Ray, P.A. Bostian, J.E. Markel, B.A. Lindsey, Highly metastatic K7M2 cell line: a novel murine model capable of in vivo imaging via luciferase vector transfection, J. Orthop. Res. 36 (8) (2018) 2296–2304.
[31] C. Chen, L. Xie, T. Ren, Y. Huang, J. Xu, W. Guo, Immunotherapy for osteosarcoma: fundamental mechanism, rationale, and recent breakthroughs, Cancer Lett. 500 (2021) 1–10.
[32] J. Liu, Z. Li, D. Zhao, X. Feng, C. Wang, D. Li, J. Ding, Immunogenic Cell Death-Inducing Chemotherapeutic Nanoformulations Potentiate Combination Chemoimmunotherapy, Materials & Design, 2021, 109465.
[33] J. Qi, W. Li, K. Lu, F. Jin, D. Liu, X. Xu, X. Wang, X. Kang, W. Wang, G. Shu, pH and thermal dual-sensitive nanoparticle-mediated synergistic antitumor effect of immunotherapy and microwave thermotherapy, Nano Lett. 19 (8) (2019) 4949–4959.
[34] J. Yu, X. He, Z. Wang, Y. Wang, S. Liu, X. Li, Y. Huang, Combining PD-L1 inhibitors with immunogenic cell death triggered by chemo-photothermal therapy via a thermosensitive liposome system to stimulate tumor-specific immunological response, Nanoscale 13 (30) (2021) 12966–12978.
[35] T. Gao, Z. Zhang, S. Liang, S. Fu, W. Mu, L. Guan, Y. Liu, Q. Chu, Y. Fang, Y. Liu, Reshaping antitumor immunity with chemo-photothermal integrated nanoplatform to augment checkpoint blockade-based cancer therapy, Adv. Funct. Mater. (2021), 2100437.
[36] J. Fucikova, E. Becht, K. Iribarren, J. Goc, R. Remark, D. Damotte, M. Alifano, P. Devi, J. Biton, C. Germain, Calreticulin expression in human Non–Small cell lung cancers correlates with increased accumulation of antitumor immune cells and favorable prognosis, Cancer Res. 76 (7) (2016) 1746–1756.
[37] R. Saenz, D. Futalan, L. Leutenez, F. Eekhout, J.F. Fecteau, S. Sundelius, S. Sundqvist, M. Larsson, T. Hayashi, B. Minev, TLR4-dependent activation of dendritic cells by an HMGB1-derived peptide adjuvant, J. Transl. Med. 12 (1) (2014) 1–11.
[38] C. Silva-Vilches, S. Ring, K. Mahnke, ATP and its metabolite adenosine as regulators of dendritic cell activity, Front. Immunol. 9 (2018) 2581.
[39] K. Pu, Y. Zhang, Transformable nanosensitizer with tumour microenvironment-activated sonodynamic process and calcium release for enhanced cancer immunotherapy, Angew. Chem., Int. Ed. Engl. 60 (25) (2021) 14051–14059.
[40] P. Matzinger, Tolerance, danger, and the extended family, Annu. Rev. Immunol. 12 (1) (1994) 991–1045.
[41] J. Wang, H. Zhang, X. Sun, X. Wang, T. Ren, Y. Huang, R. Zhang, B. Zheng, W. Guo, Exosomal PD-L1 and N-cadherin predict pulmonary metastasis progression for osteosarcoma patients, J. Nanobiotechnol. 18 (1) (2020) 1–23.
[42] Z. Li, H. Cai, Z. Li, L. Ren, X. Ma, H. Zhu, Q. Gong, H. Zhang, Z. Gu, K. Luo, A tumor cell membrane-coated self-amplified nanosystem as a nanovaccine to boost the therapeutic effect of anti-PD-L1 antibody, Bioact. Mater. 21 (2023) 299–312.
[43] K. Rangamuwa, T. Leong, S. Bozinovski, M. Christie, T. John, P. Antippa, L. Irving, D. Steinfort, Increase in tumour PD-L1 expression in non-small cell lung cancer following bronchoscopic thermal vapour ablation, Transl. Lung Cancer Res. 10 (6) (2021) 2858–2864.
[44] L. Shi, L. Chen, C. Wu, Y. Zhu, B. Xu, X. Zheng, M. Sun, W. Wen, X. Dai, M. Yang, Q. Lv, B. Lu, J. Jiang, PD-1 blockade boosts radiofrequency ablation-elicited adaptive immune responses against tumor, clinical cancer research : an, official journal of the American Association for Cancer Research 22 (5) (2016) 1173–1184.
[45] L. Huang, Y. Li, Y. Du, Y. Zhang, X. Wang, Y. Ding, X. Yang, F. Meng, J. Tu, L. Luo, C. Sun, Mild photothermal therapy potentiates anti-PD-L1 treatment for immunologically cold tumors via an all-in-one and all-in-control strategy, Nat. Commun. 10 (1) (2019) 4871.
[46] D.M. Lussier, L. O'Neill, L.M. Nieves, M.S. McAfee, S.A. Holechek, A.W. Collins, P. Dickman, J. Jacobsen, P. Hingorani, J.N. Blattman, Enhanced T-cell immunity to osteosarcoma through antibody blockade of PD-1/PD-L1 interactions, J. Immunother. 38 (3) (2015) 96–106.
[47] Y. Mochizuki, H. Tazawa, K. Demiya, M. Kure, H. Kondo, T. Komatsubara, K. Sugiu, J. Hasei, A. Yoshida, T. Kunisada, Y. Urata, S. Kagawa, T. Ozaki, T. Fujiwara, Telomerase-specific oncolytic immunotherapy for promoting efficacy of PD-1 blockade in osteosarcoma, Cancer immunology, immunotherapy, CII 70 (5) (2021) 1405–1417.
[48] S. Jhunjhunwala, C. Hammer, L. Delamarre, Antigen presentation in cancer: insights into tumour immunogenicity and immune evasion, Nat. Rev. Cancer 21 (5) (2021) 298–312.
[49] A. Giatromanolaki, I. Anestopoulos, M.I. Panayiotidis, A. Mitrakas, A. Pappa, M. I. Koukourakis, Prognostic relevance of the relative presence of CD4, CD8 and CD20 expressing tumor infiltrating lymphocytes in operable non-small cell lung cancer patients, Anticancer Res. 41 (8) (2021) 3989–3995.
[50] L. Federico, D.J. McGrail, S.E. Bentebibel, C. Haymaker, A. Ravelli, M.A. Forget, T. Karpinets, P. Jiang, A. Reuben, M.V. Negrao, J. Li, R. Khairullah, J. Zhang, A. Weissferdt, A.A. Vaporciyan, M.B. Antonoff, G. Walsh, S.Y. Lin, A. Futreal, I. Wistuba, J. Roth, L.A. Byers, P.O. Gaudreau, N. Uraoka, A.F. Cruz, H. Dejima, R. N. Lazcano, L.M. Solis, E.R. Parra, J.J. Lee, S. Swisher, T. Cascone, J.V. Heymach, J. Zhang, B. Sepesi, D.L. Gibbons, C. Bernatchez, Distinct tumor-infiltrating lymphocyte landscapes are associated with clinical outcomes in localized non-small-cell lung cancer, Ann. Oncol. : official journal of the European Society for Medical Oncology 33 (1) (2022) 42–56.
[51] T. Fujiwara, M.A. Yakoub, A. Chandler, A.B. Christ, G. Yang, O. Ouerfelli, V. K. Rajasekhar, A. Yoshida, H. Kondo, T. Hata, H. Tazawa, Y. Dogan, M.A.S. Moore, T. Fujiwara, T. Ozaki, E. Purdue, J.H. Healey, CSF1/CSF1R signaling inhibitor pexidartinib (PLX3397) reprograms tumor-associated macrophages and stimulates T-cell infiltration in the sarcoma microenvironment, Mol. Cancer Therapeut. 20 (8) (2021) 1388–1399.
[52] B. Li, X. Zhu, L. Sun, L. Yuan, J. Zhang, H. Li, Z. Ye, Induction of a specific CD8+ T-cell response to cancer/testis antigens by demethylating pre-treatment against osteosarcoma, Oncotarget 5 (21) (2014) 10791–10802.
[53] M. Poggio, T. Hu, C.C. Pai, B. Chu, C.D. Belair, A. Chang, E. Montabana, U.E. Lang, Q. Fu, L. Fong, R. Blelloch, Suppression of exosomal PD-L1 induces systemic anti-tumor immunity and memory, Cell 177 (2) (2019) 414–427, e13.
[54] I. Rousalova, E. Krepela, Granzyme B-induced apoptosis in cancer cells and its regulation (review), Int. J. Oncol. 37 (6) (2010) 1361–1378.
[55] Z.-W. Luo, P.-P. Liu, Z.-X. Wang, C.-Y. Chen, H. Xie, Macrophages in osteosarcoma immune microenvironment: implications for immunotherapy, Front. Oncol. 10 (2020).
[56] S. Yoshizawa, A. Brown, A. Barchowsky, C. Sfeir, Magnesium ion stimulation of bone marrow stromal cells enhances osteogenic activity, simulating the effect of magnesium alloy degradation, Acta Biomater. 10 (6) (2014) 2834–2842.
[57] Y. Wang, Z. Geng, Y. Huang, Z. Jia, Z. Cui, Z. Li, S. Wu, Y. Liang, S. Zhu, X. Yang, Unraveling the osteogenesis of magnesium by the activity of osteoblasts in vitro, J. Mater. Chem. B 6 (2018).
[58] H. Naujokat, A. Gülses, J.R. Wiltfang, Y. Açil, Effects of degradable osteosynthesis plates of MgYREZr alloy on cell function of human osteoblasts, fibroblasts and osteosarcoma cells, J. Mater. Sci. Mater. Med. 28 (8) (2017) 126.
[59] L.-A. D, M. L, B. P, P. E, V. K, B. M, M. D, P. H, PH IN the engineered microenvironment: a critical factor for optimal osteogenesis mediated by human mesenchymal stem cell, Orthopaedic Proceedings 96-B (SUPP_11) (2014), 118-118.
[60] J.P. Johnson, C.T. Born, N. Thomas, J. Truntzer, P.K. Mansuripur, J. Kleiner, S. T. McAlister, D. Garcia, S. Koruprolu, Development of a novel murine femur fracture and fixation model, J. Orthop. 17 (2020) 162–167.